

Optimal control of differentially flat underactuated planar robots in the perspective of oscillation mitigation

Stefano Lovato¹, Michele Tonan¹, Matteo Bottin¹, Matteo Massaro¹, Alberto Doria¹, Giulio Rosati¹

Abstract—Underactuated robots are characterized by a larger number of degrees of freedom than actuators and if they are designed with a specific mass distribution, they can be controlled by means of differential flatness theory. This structural property enables the development of lightweight and cost-effective robotic systems with enhanced dexterity. However, a key challenge lies in managing the passive joints, whose control demands precise and comprehensive dynamic modeling of the system. To simplify dynamic models, particularly for low-speed trajectories, friction is often neglected. While this assumption simplifies analysis and control design, it introduces residual oscillations of the end-effector about the target position. In this paper, the possibility of using optimal control along with differential flatness control is investigated to improve the tracking of the planned trajectories. First, the study was carried out through formal analysis, and then, it was validated by means of numerical simulations.

Results highlight that optimal control can be used to plan the flat variables considering different (quadratic) performance indices: control effort, i.e. motor torque, and potential energy of the considered underactuated joint. Moreover, the minimization of potential energy can be used to design motion laws that are robust against variation of the stiffness and damping of the underactuated joint, thus reducing oscillations in the case of stiffness/damping mismatch.

I. INTRODUCTION

Underactuated systems are dynamic systems with some joints without direct actuation, and the links are connected via elastic elements to the rest of kinematic chain. In such systems, actuated joints indirectly control the motion of the elastic joints.

Research in this area has expanded, leading to applications such as jointed arm robots [1], [2], [3], cable-driven robots [4], [5], and walking robots [6], [7]. These systems are attractive for their reduced weight and cost, and increased dexterity with fewer actuators [8], [9]. Other notable examples include prosthetic devices [10], sea surface robots [11], and advanced grippers [12], [13], [14].

However, underactuated systems are hard to control, and over the years, many solutions have been proposed to overcome their limitations [15], [16]. Differential flatness, a property allowing system states to be expressed via flat outputs thanks to specific inertial properties [17], [18], has facilitated control strategies for both linear and nonlinear systems [19], [20], [21], [22]. For underactuated robots, flatness-based control has been validated in simulations and experiments,

both for point-to-point and more complex motions [23], [24], [25], [26]. During the years, disturbances such as friction have been included in the mathematical model [27].

Robot trajectories, whether for fully actuated or underactuated systems, can be optimized with respect to various performance criteria, such as minimizing motion time [28] or reducing energy consumption [29]. Within the framework of differentially flat systems, researchers showed that optimal control methods can be adopted to plan feasible trajectories [30]. Further comparative studies evaluated the effectiveness of Linear Quadratic Regulator (LQR) control against differentially flat control strategies, particularly in applications involving linear guide feedback systems [31].

This paper focuses on how optimal control can be used in the trajectory planning of underactuated differentially flat planar robots to achieve better performance in terms of control effort, i.e. motor torque, or oscillation mitigation at the end of the motion. The paper is structured as follows. Section II presents the mathematical model of serial differential flat robots. Section III describes the optimal control planning strategies. Section IV shows some simulations and describes the results. Section V draws the conclusions.

II. MATHEMATICAL MODEL

The robot considered in this paper presents one passive joint and is differentially flat since it is designed according to [23]. In particular, a n -DOF robot with only one passive joint is differentially flat if the center of mass of the final link (n) is on the n -th joint axis and if the center of mass of both links n and $n - 1$ is on the $(n - 1)$ -th joint axis. The actuators for the system are located on all joints but the last, which is equipped with a torsional spring of stiffness k_n and a viscous damper with damping coefficient c_n .

Figure 1 shows the scheme of an n -DOF robot with the last passive joint. q_1 represents the rotation of link 1 with respect to the base frame $x - y$, and q_i is the relative rotation of link i with respect to $i - 1$ link. Mass and barycentric moment of inertia of the i -th link are m_i and I_{G_i} , respectively; the distance of the center of mass of i -th link from the i -th joint and the link total length are a_{G_i} and a_i respectively (please note that $a_{G(n-1)} = a_{G_n} = 0$ since the two links are fully balanced). The last two fully balanced links are equipped with two counterbalancing masses, namely $m_{c(n-1)}$ and $m_{c(n)}$, placed at a distance $a_{C(n-1)}$ and $a_{C(n)}$ from the respective joint.

The dynamic model of the system can be derived by means of the Lagrangian approach in matrix form:

$$\mathbf{M}_n(\mathbf{q})\ddot{\mathbf{q}} + \mathbf{C}_n\dot{\mathbf{q}} + \mathbf{K}_n\mathbf{q} + \mathbf{b}(\mathbf{q}, \dot{\mathbf{q}}) + \mathbf{g}(\mathbf{q}) = \boldsymbol{\tau} \quad (1)$$

Project financially supported by BIRD 2023 Research Program of University of Padova grant number BOTT_BIRD23.01.

¹All the authors are with the Department of Industrial Engineering, University of Padova, Via Venezia 1, Padova, Italy matteo.bottin@unipd.it

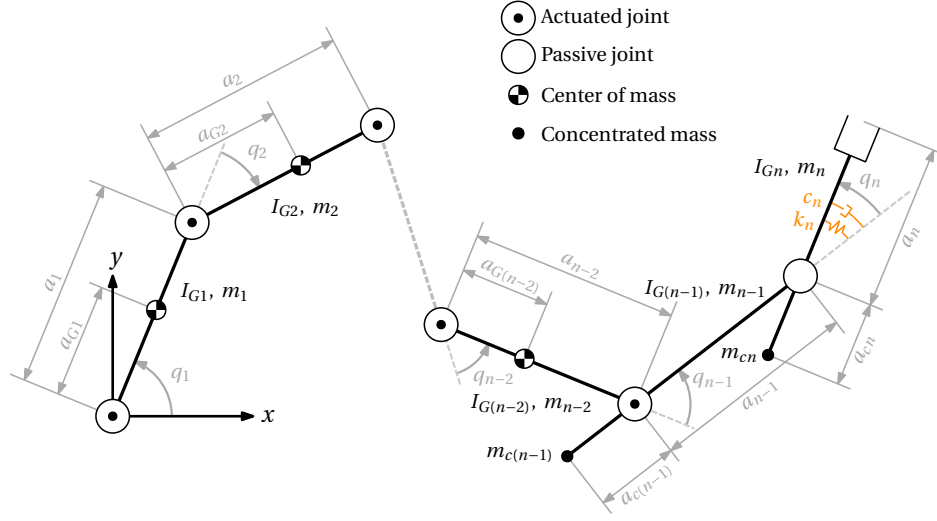


Fig. 1. Scheme of the underactuated differentially flat robot with n -DOF.

where \mathbf{q} , $\dot{\mathbf{q}}$ and $\ddot{\mathbf{q}}$ contain all joint variables and their first and second derivatives, $\mathbf{b}(\mathbf{q}, \dot{\mathbf{q}})$ contains all Coriolis-centrifugal terms and $\mathbf{g}(\mathbf{q})$ contains all gravitational terms. Please note that the last two terms of both $\mathbf{b}(\mathbf{q}, \dot{\mathbf{q}})$ and $\mathbf{g}(\mathbf{q})$ are null since the links are fully balanced. \mathbf{M}_n , \mathbf{C}_n and \mathbf{K}_n are the mass, damping, and stiffness matrices, defined as:

$$\mathbf{M}_n(\mathbf{q}) = \begin{bmatrix} & I_{n-1}^* & I_n^* \\ & I_{n-1}^* & I_n^* \\ \mathbf{I}_{(n-2) \times (n-2)}^*(\mathbf{q}) & \vdots & \vdots \\ I_{n-1}^* & \cdots & I_{n-1}^* \\ I_n^* & \cdots & I_n^* \end{bmatrix}$$

$$\mathbf{C}_n = \begin{bmatrix} 0 & & & \\ \mathbf{0}_{(n-1) \times (n-1)} & \vdots & & \\ & 0 & & \\ 0 & \cdots & 0 & c_n \end{bmatrix}, \quad \mathbf{K}_n = \begin{bmatrix} 0 & & & \\ \mathbf{0}_{(n-1) \times (n-1)} & \vdots & & \\ & 0 & & \\ 0 & \cdots & 0 & k_n \end{bmatrix} \quad (2)$$

It is worth noting that the last two rows of matrix \mathbf{M}_n are constant, i.e., are independent for any robot configuration \mathbf{q} . From Eq.(2) differential flatness can be used to define a set of flat variables $\mathbf{y}(t)$ so that:

$$y_1 = \sum_{i=1}^n q_i, \quad y_k = q_{k-1} \text{ with } k = 2, \dots, n-1 \quad (3)$$

where y_1 has the physical meaning of absolute orientation of the last link with respect to the fixed reference frame.

Exploiting the flat variables, the motion of the last joint can be controlled [32]:

$$q_n = -\frac{I_n^*}{k_n} \ddot{y}_1 + \frac{I_n^* c_n}{k_n^2} y_1 \quad (3)$$

$$\ddot{q}_n = -\frac{I_n^*}{k_n} y_1^{(4)} + \frac{I_n^* c_n}{k_n^2} y_1^{(5)} \quad (4)$$

with the motor torque τ_{n-1} of joint $n-1$ given by:

$$\tau_{n-1} = I_{n-1}^* \ddot{y}_1 + \frac{I_n^* (I_{n-1}^* - I_n^*)}{k_n} y_1^{(4)} - \frac{I_n^* (I_{n-1}^* - I_n^*) c_n}{k_n^2} y_1^{(5)} \quad (5)$$

where $y_1^{(i)} = \frac{d^i y_1}{dt^i}$ is the i -th time derivative of y_1 .

The control of q_n can be achieved by a proper planning of the flat variable y_1 . In particular, it is important to notice that the dynamic model contains the acceleration (Eq.(2)), hence the flat variable y_1 must be a C^5 function, and 6 conditions must be imposed on both the initial and final configurations, for a total of 12 boundary conditions. Such conditions are the initial and final joint angles, as well as the null derivatives. Additional constraints can be imposed if there is the need for passing through viapoints [32].

It is worth noting that Eq.(5) is achieved by employing a Taylor expansion that implies a small approximation, thus the analytical result is not exact, and some oscillations may appear which result in small errors at the end of the motion [27].

III. OPTIMAL MOTION PLANNING

Previous work [32] has shown that in order to enforce the 12 boundary conditions, an 11th degree polynomial is sufficient to ensure a C^5 function for the flat variable y_1 . Nevertheless, adopting a different motion law for y_1 can be advantageous when the objective is to optimize other factors in the trajectory, such as the control effort.

In this section, a more general framework for motion planning is presented, which is based upon the Euler-Lagrange equation (ELE) [33] applied to a quadratic performance index. The cost function \mathcal{J} is assumed to be of the form

$$\mathcal{J}[y_1(t)] = \int_{t_i}^{t_f} \mathcal{L}(y_1^{(1)}, \dots, y_1^{(6)}) dt = \int_0^T \frac{1}{2} (\mathbf{y}_1)^T \mathbf{Q}(\mathbf{y}_1) dt \quad (6)$$

where t_i, t_f are the initial and final motion times, \mathcal{L} is the integral cost, $\mathbf{y}_1 = [y_1^{(1)}, y_1^{(2)}, \dots, y_1^{(6)}]^T$ is a vector containing the flat variable derivatives from order 1 to order 6, and $\mathbf{Q} = [q_{ij}]$ is a 6×6 symmetric positive-semidefinite weighting matrix. The ELE for an integral cost including derivatives up to 6-th order is

$$\sum_{k=0}^6 (-1)^k \frac{d^k}{dt^k} \left(\frac{\partial \mathcal{L}}{\partial y_1^{(k)}} \right) = 0 \quad (7)$$

which applied to Eq.(6) gives the following 12-order constant-coefficient linear ordinary differential equation

$$\begin{aligned} & q_{66}y_1^{(12)} - (q_{55} - 2q_{64})y_1^{(10)} + (q_{44} - 2q_{53} + 2q_{62})y_1^{(8)} \\ & - (q_{33} + 2q_{51} - 2q_{42})y_1^{(6)} + (q_{22} - 2q_{31})y_1^{(4)} - q_{11}y_1^{(2)} = 0 \end{aligned} \quad (8)$$

The solution of Eq.(8) is obtained by studying the roots of the corresponding characteristic polynomial. Real roots are associated with solutions of the type

$$y_1(t) = e^{\beta t} \sum_{k=0}^{m-1} C_k t^k \quad (9)$$

where β is the root and m its multiplicity. Pair complex conjugate roots are associated with solutions of the type

$$y_1(t) = e^{\alpha t} \left[\left(\sum_{k=0}^{m-1} A_k t^k \right) \cos \omega t + \left(\sum_{k=0}^{m-1} B_k t^k \right) \sin \omega t \right] \quad (10)$$

where α, ω are the real and imaginary parts of the root, respectively. The general solution is obtained by combining the solution bases and involves 12 coefficients (C_k and/or A_k, B_k), which are obtained by enforcing the 12 boundary conditions.

Depending on the selected performance index, different motion laws $y_1(t)$ are obtained. In this work, three performance indexes are separately considered.

A. Polynomial planning

The first performance index aims to minimize the RMS value of $y_1^{(6)}$, to give the polynomial planning used in [32]. The integral cost \mathcal{L} is

$$\mathcal{L} = (y_1^{(6)})^2 \quad (11)$$

which means $q_{66} = 1$ and the other coefficients of \mathbf{Q} are null. In such a case, Eq.(8) reduces to

$$y_1^{(12)} = 0 \quad (12)$$

whose solution is a 11-th degree polynomial.

B. Min-control-effort planning

The second performance index considered aims to minimize the control effort, represented by the motor torque τ_{n-1} . In this case, the integral cost \mathcal{L} is a combination of $(y_1^{(6)})^2$ and $(\tau_{n-1})^2$ and is given by

$$\mathcal{L} = (y_1^{(6)})^2 + r^8 \left[\tau_{n-1} \left(\ddot{y}_1, (y_1^{(4)}), (y_1^{(5)}) \right) \right]^2 \quad (13)$$

where r is weighting factor used to tune the minimization¹.

The coefficients in Eq.(8) are

$$\begin{aligned} q_{22} &= r^8 I_{n-1}^{*2} \\ q_{42} &= r^8 \frac{I_{n-1}^* I_n^* (I_{n-1}^* - I_n^*)}{k_n} \\ q_{44} &= r^8 \frac{I_n^{*2} (I_{n-1}^* - I_n^*)^2}{k_n^2} \\ q_{52} &= r^8 \frac{c_n I_{n-1}^* I_n^* (I_{n-1}^* - I_n^*)}{k_n^2} \\ q_{54} &= r^8 \frac{c_n I_n^{*2} (I_{n-1}^* - I_n^*)^2}{k_n^3} \\ q_{55} &= r^8 \frac{c_n^2 I_n^{*2} (I_{n-1}^* - I_n^*)^2}{k_n^4} \\ q_{66} &= 1 \end{aligned} \quad (14)$$

It is worth noting that when $r \rightarrow \infty$, Eq.(8) becomes a 10-order ordinary differential equation, with only 10 coefficients being determined by the boundary conditions. In such case, not all the specified boundary conditions can be arbitrarily enforced.

C. Min-potential-energy planning

The third performance index introduced aims to minimize the potential energy $U_n = \frac{1}{2} k_n q_n^2$ accumulated in the underactuated joint. This objective is motivated by the desire of reducing the influence of the joint stiffness and damping (i.e. k_n, c_n) on the actual motion of the system. Using the flat variables, the motion of the last joint q_n is expressed as a function of $\ddot{y}_1, y_1^{(3)}$; see Eq.(4). Under the assumption of small c_n , the dominant contribution is given by \ddot{y}_1 . Consequently, to minimize the potential energy U_n , the selected integral cost is a combination of $(y_1^{(6)})^2$ and $(\ddot{y}_1)^2 \propto U_n$ and is defined as

$$\mathcal{L} = (y_1^{(6)})^2 + p^8 \ddot{y}_1^2 \quad (15)$$

where p is weighting factor used to tune the minimization². It yields:

$$y_1^{(12)} - p^8 y_1^{(4)} = 0 \quad (16)$$

A closed-form solution exists in this case and is

$$\begin{aligned} y_1(t) &= C_1 + C_2 t + C_3 t^2 + C_4 t^3 \\ &+ e^{\frac{\sqrt{2+\sqrt{2}}}{2} pt} \left[A_1 \cos \left(\frac{\sqrt{2+\sqrt{2}}}{2} pt \right) + B_1 \sin \left(\frac{\sqrt{2+\sqrt{2}}}{2} pt \right) \right] \\ &+ e^{\frac{\sqrt{2-\sqrt{2}}}{2} pt} \left[A_2 \cos \left(\frac{\sqrt{2+\sqrt{2}}}{2} pt \right) + B_2 \sin \left(\frac{\sqrt{2+\sqrt{2}}}{2} pt \right) \right] \\ &+ e^{\frac{\sqrt{2+\sqrt{2}}}{2} pt} \left[A_3 \cos \left(\frac{\sqrt{2-\sqrt{2}}}{2} pt \right) + B_3 \sin \left(\frac{\sqrt{2-\sqrt{2}}}{2} pt \right) \right] \\ &+ e^{\frac{\sqrt{2-\sqrt{2}}}{2} pt} \left[A_4 \cos \left(\frac{\sqrt{2-\sqrt{2}}}{2} pt \right) + B_4 \sin \left(\frac{\sqrt{2-\sqrt{2}}}{2} pt \right) \right] \end{aligned} \quad (17)$$

¹It is worth noting that r and p are elevated to the power of 8 so that the values of r and p can be chosen below 1000. In other words, the power of 8 acts only as a scaling factor, and has no physical meaning.

²See footnote 1

with the 12 coefficients $C_1, \dots, C_4, A_1, \dots, A_4, B_1, \dots, B_4$ determined by the boundary conditions. When $p \rightarrow \infty$, Eq.(16) becomes

$$y_1^{(4)} = 0 \quad (18)$$

whose solution is a 3-th degree polynomial, with only 4 coefficients being determined by the boundary conditions. Again, not all the specified boundary conditions can be arbitrarily enforced in this case.

As a final remark, motion planning with mixed-minimization can also be considered, i.e. Eq.(13) together with (15). The corresponding integral cost is

$$\mathcal{L} = (y_1^{(6)})^2 + r^8 \left[\tau_{n-1} \left(\ddot{y}_1, (y_1^{(4)}), (y_1^{(5)}) \right) \right]^2 + p^8 \ddot{y}_1^2 \quad (19)$$

which gives the same coefficients of Eq.(14) with the only exception of q_{22} which is:

$$q_{22} = r^8 I_{n-1}^{*2} + p^8 \quad (20)$$

IV. EXAMPLE OF APPLICATION ON A 2-DOF UNDERACTUATED ROBOT

The proposed optimal motion planning is applied to a planar 2-DOF robot with one motor and one underactuated joint. The robot consists of two links, with the second one fully balanced. The joint variables are $\mathbf{q} = [q_1, q_2]^T$, the matrices in Eq.(2) are

$$\mathbf{M}_n = \begin{bmatrix} I_1^* & I_2^* \\ I_2^* & I_2^* \end{bmatrix}, \quad \mathbf{C}_n = \begin{bmatrix} 0 & 0 \\ 0 & c_2 \end{bmatrix}, \quad \mathbf{K}_n = \begin{bmatrix} 0 & 0 \\ 0 & k_2 \end{bmatrix} \quad (21)$$

and only one flat variable $y_1 = q_1 + q_2$ is required. The relationships between y_1 and q_2 and their derivatives are

$$\begin{aligned} q_2 &= -\frac{I_2^*}{k_2} \ddot{y}_1 + \frac{I_2^* c_2}{k_2^2} y_1^{(3)} \\ \ddot{q}_2 &= -\frac{I_2^*}{k_2} y_1^{(4)} + \frac{I_2^* c_2}{k_2^2} y_1^{(5)} \end{aligned} \quad (22)$$

The approximated motor torque τ_1 of the first joint is given by Eq.(5) and becomes

$$\tau_1 = I_1^* \ddot{y}_1 + \frac{I_2^* (I_1^* - I_2^*)}{k_2} y_1^{(4)} - \frac{I_2^* (I_1^* - I_2^*) c_2}{k_2^2} y_1^{(5)} \quad (23)$$

The 12 boundary conditions at the beginning (t_i) and the end (t_f) of the motion are

$$\begin{cases} y_1(t_i) = q_{1i} + q_{2i} \\ y_1(t_f) = q_{1f} + q_{2f} \\ y_1^{(i)}(t_i) = 0 \quad \forall i = 1, 2, \dots, 5 \\ y_1^{(i)}(t_f) = 0 \quad \forall i = 1, 2, \dots, 5 \end{cases} \quad (24)$$

where q_{1i}, q_{2i} and q_{1f}, q_{2f} are the initial and final angular positions of joints 1 and 2, respectively.

Three scenarios are considered, with a target motion having $q_{1i} = q_{2i} = 0$ at $t_i = 0$ and $q_{1f} = \pi, q_{2f} = 0$ at $t_f = 1$ s³. For each scenario, the motion is planned using the

³Please note that in a point-to-point motion $q_{2i} = q_{2f} = 0$; otherwise, the robot could not hold the initial and final positions with null velocities and accelerations due to the spring placed in the second joint [26].

TABLE I
2-DOF ROBOT PARAMETERS.

Parameter	Value	Unit
I_1^*	$6.4 \cdot 10^{-4}$	kgm ²
I_2^*	$3.3 \cdot 10^{-5}$	kgm ²
k_2	$3 \cdot 10^{-3}$	Nm/rad
c_2	$2 \cdot 10^{-5}$	Nms/rad

polynomial law, the min-control-effort strategy with $r = 150$, and the min-potential-energy strategy with $p = 17$, to give the planned flat variable $y_1(t)$. For each motion-planning strategy, the corresponding joint 1 torque τ_1 is calculated using Eq.(23). Finally, the dynamic model in Eq.(1) with the system matrices in Eq.(21) is simulated using τ_1 as a feed-forward torque, in order to compare the actual motion of the robot to the planned one. The employed robot dataset is reported in Table (I). Results are summarized in Table (II) and will be commented in the following sections. The free oscillation after the motion (i.e. $t \geq t_f$) is evaluated from its initial amplitude at the end of the motion (t_f):

$$A = \sqrt{q_2^2(t_f) + \frac{I_2^*}{k_2} \dot{q}_2^2(t_f)} \quad (25)$$

A. Scenario 1

In the first scenario, no damping is considered (i.e. $c_2 = 0$), and exactly the same c_2, k_2 are employed in both the motion planning and simulated model. Figure 2 shows the

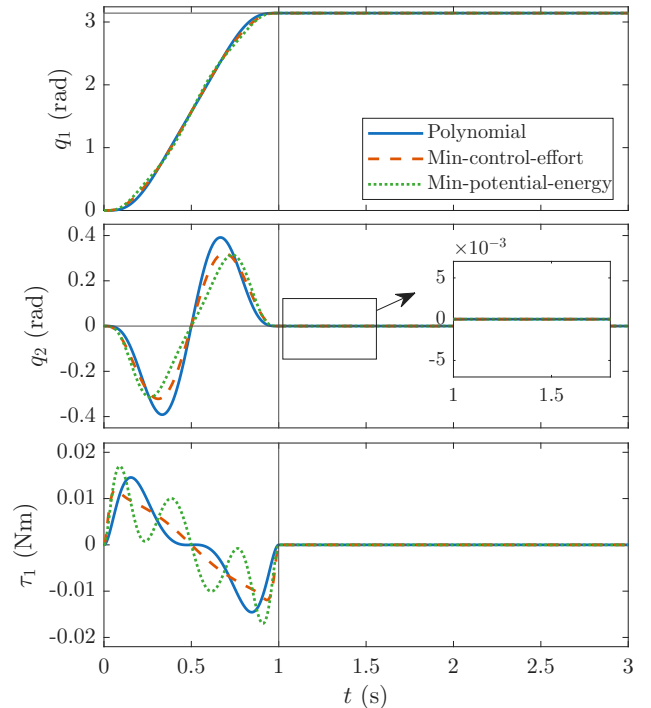


Fig. 2. Angular positions of joint 1 (top) and 2 (middle) and joint 1 torque (bottom) obtained for scenario 1. The vertical solid line denotes the end of the motion.

simulated q_1, q_2 (top and middle), along with the joint 1 torque τ_1 (bottom). The RMS of the joint 1 torque is 0.0074 Nm for the polynomial motion planning (solid blue). Not surprisingly, this reduces to 0.0069 Nm (-6.8%) when using the min-control-effort strategy (dashed red). When the motion is planned using the min-potential-energy strategy (dotted green), the RMS of the joint 1 torque again increases to 0.0087 Nm (+18%), with a more oscillating control during the motion. In all cases, at the end of the motion (vertical solid line) no oscillations are observed in q_1, q_2 , as Eq.(23) is exact for $c_2 = 0$ and the same c_2, k_2 are employed in both the motion planning and simulated model.

B. Scenario 2

In the second scenario, damping is included (i.e. $c_2 > 0$), again with both motion planning and simulated model using the same c_2, k_2 . The results are depicted in Figure 3.

In this case, the RMS of the joint 1 torque is 0.0068 Nm, 0.0064 Nm (-5.9%), and 0.0079 Nm (+16%) for the motion planned using the polynomial, the min-control-effort strategy, and the min-potential-energy strategy, respectively. Again, a lower RMS torque is observed with the min-control-effort strategy, whereas torque oscillations occur with the min-potential-energy strategy. As Eq.(23) is approximated when $c_2 \neq 0$, oscillations are clearly observed in q_2 . The initial amplitude of the oscillation in q_2 is 0.0045 rad with the polynomial planning. The value reduces to 0.0036 rad (-20%) when the min-control-effort strategy is used. The reduction is even more significant when the min-potential-energy strategy is adopted, with an oscillation amplitude of 0.003 rad (-35%).

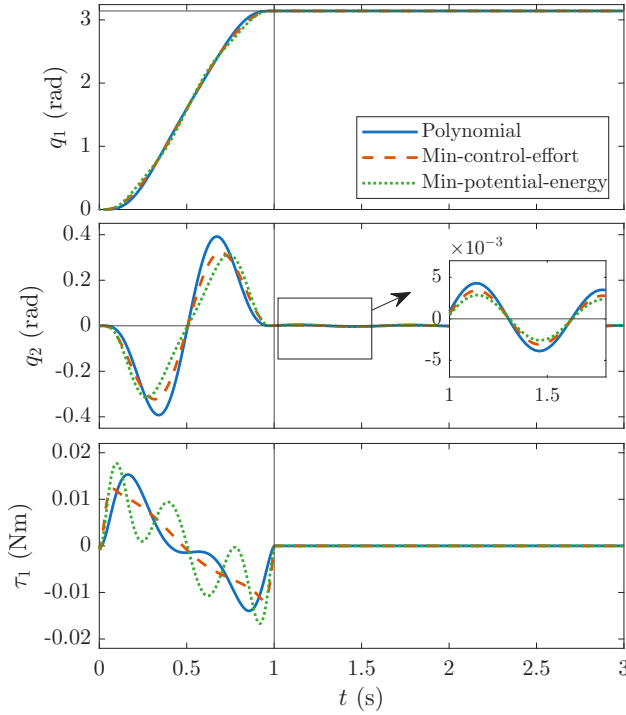


Fig. 3. Angular positions of joint 1 (top) and 2 (middle) and joint 1 torque (bottom) obtained for scenario 2. The vertical solid line denotes the end of the motion.

TABLE II

RESULTS FOR THE THREE SIMULATED SCENARIOS. THE PERCENTAGES REFER TO THE POLYNOMIAL STRATEGY OF THE SAME SCENARIO.

Scenario	Strategy	Torque RMS (Nm)	A (rad)
1	Polynomial	0.0074	0
	Min-control	0.0069 (-6.8%)	0
	Min-potential	0.0087 (+18%)	0
2	Polynomial	0.0068	0.0045
	Min-control	0.0064 (-5.9%)	0.0036 (-20%)
	Min-potential	0.0079 (+16%)	0.003 (-35%)
3	Polynomial	0.0068	0.099
	Min-control	0.0064 (-5.9%)	0.077 (-22%)
	Min-potential	0.0079 (+16%)	0.062 (-38%)

C. Scenario 3

In the third scenario, a mismatch of c_2, k_2 between the motion planning and simulated model is considered. In particular, the damping c_2 and stiffness k_2 are both increased by 10% in the perturbed system. The results are shown in Figure 4. The joint 1 torque remains exactly the same of scenario 2, since the motion is planned with exactly the same c_2, k_2 . However, when the control is applied to the perturbed system, larger oscillations are clearly observed in q_2 due to the mismatch of c_2, k_2 . The amplitude of the oscillation in q_2 is 0.099 rad with the polynomial planning, which is reduced to 0.077 rad (-22%) when the min-potential-energy strategy is employed. Again, the reduction is even more significant when using the min-potential-energy strategy, with an oscillation amplitude of 0.062 rad (-38%).

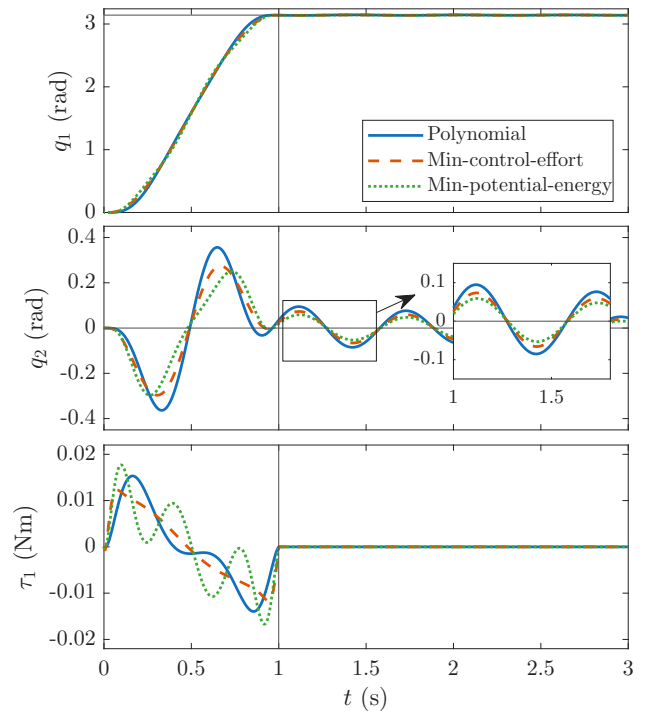


Fig. 4. Angular positions of joint 1 (top) and 2 (middle) and joint 1 torque (bottom) obtained for scenario 3. The vertical solid line denotes the end of the motion.

V. CONCLUSIONS

The differential flatness theory can be used to perform point-to-point motions for underactuated serial robots with specific mass distribution. However, in its standard form the trajectory planning is performed by means of high-degree polynomials, whereas the equations do not require such a specific planning function.

Hence, optimal control can be employed to enforce the required boundary conditions while at the same time optimizing other factors in the trajectory.

Results have shown that optimal control can provide better performance for differentially flat underactuated robot in terms of torque RMS (in the case of the minimal control effort planning strategy) and in terms of oscillation amplitude at the end of the motion (in the case of the minimal potential energy planning strategy). A combination of these two strategies can be employed using specific weighting factors.

REFERENCES

- [1] S. K. Agrawal and V. Sangwan, "Design of under-actuated open-chain planar robots for repetitive cyclic motions," in *International Design Engineering Technical Conferences and Computers and Information in Engineering Conference*, vol. 42568, pp. 1057–1066, 2006.
- [2] A. Firouzeh, S. S. M. Salehian, A. Billard, and J. Paik, "An under actuated robotic arm with adjustable stiffness shape memory polymer joints," in *2015 IEEE International Conference on Robotics and Automation (ICRA)*, pp. 2536–2543, IEEE, 2015.
- [3] G. Qin, A. Ji, Y. Cheng, W. Zhao, H. Pan, S. Shi, and Y. Song, "Design and motion control of an under-actuated snake arm maintainer," *Robotica*, vol. 40, no. 6, pp. 1763–1782, 2022.
- [4] L. Barbazza, D. Zanotto, G. Rosati, and S. Agrawal, "Design and optimal control of an underactuated cable-driven micro-macro robot," *IEEE Robotics and Automation Letters*, vol. 2, no. 2, pp. 896–903, 2017.
- [5] D. Zanotto, G. Rosati, and S. K. Agrawal, "Modeling and control of a 3-dof pendulum-like manipulator," in *2011 IEEE International Conference on Robotics and Automation*, pp. 3964–3969, IEEE, 2011.
- [6] S. Gupta and A. Kumar, "A brief review of dynamics and control of underactuated biped robots," *Advanced Robotics*, vol. 31, no. 12, pp. 607–623, 2017.
- [7] B. He, S. Wang, and Y. Liu, "Underactuated robotics: a review," *International Journal of Advanced Robotic Systems*, vol. 16, no. 4, p. 1729881419862164, 2019.
- [8] M. Bottin, G. Boschetti, and G. Rosati, "A novel collision avoidance method for serial robots," *Mechanisms and Machine Science*, vol. 66, pp. 293–301, 2019.
- [9] M. Tonan, A. Doria, M. Bottin, and G. Rosati, "Influence of joint stiffness and motion time on the trajectories of underactuated robots," *Applied Sciences*, vol. 13, no. 12, p. 6939, 2023.
- [10] K. Loutan Jr and U. Persad, "The design of a low-cost voluntary closing finger prosthetic for developing countries," in *International Design Engineering Technical Conferences and Computers and Information in Engineering Conference*, vol. 87295, p. V002T02A086, American Society of Mechanical Engineers, 2023.
- [11] M. Angelini, E. Ida', D. Bertin, M. Carricato, E. Mantovani, D. Bazzi, and V. Orassi, "An underactuated cable-driven parallel robot for marine automated launch and recovery operations," in *International Design Engineering Technical Conferences and Computers and Information in Engineering Conference*, vol. 87363, p. V008T08A056, American Society of Mechanical Engineers, 2023.
- [12] J. Becedas, I. Payo, and V. Feliu, "Two-flexible-fingers gripper force feedback control system for its application as end effector on a 6-dof manipulator," *IEEE Transactions on Robotics*, vol. 27, no. 3, pp. 599–615, 2011.
- [13] B. Okken, J. P. Dekker, J. J. de Jong, and D. M. Brouwer, "Numerical optimization of underactuated flexure-based grippers," in *International Design Engineering Technical Conferences and Computers and Information in Engineering Conference*, vol. 87363, p. V008T08A041, American Society of Mechanical Engineers, 2023.
- [14] R. R. Ma, N. Rojas, and A. M. Dollar, "Spherical hands: Toward underactuated, in-hand manipulation invariant to object size and grasp location," *ASME Journal of Mechanisms and Robotics*, vol. 8, no. 6, p. 061021, 2016.
- [15] J. Bettega, D. Richiedei, I. Tamellin, and A. Trevisani, "Stable inverse dynamics for feedforward control of nonminimum-phase underactuated systems," *ASME Journal of Mechanisms and Robotics*, vol. 15, no. 3, p. 031002, 2023.
- [16] X. Xin, Z. Wang, and Y. Liu, "Parameterization of minimal order strongly stabilizing controllers for two-link underactuated planar robot with single sensor," *Automatica*, vol. 158, p. 111280, 2023.
- [17] H. Sira-Ramirez and S. K. Agrawal, *Differentially flat systems*. Crc Press, 2018.
- [18] R. M. Murray, M. Rathinam, and W. Sluis, "Differential flatness of mechanical control systems: A catalog of prototype systems," in *ASME international mechanical engineering congress and exposition*, vol. 57-1, pp. 349–357, Citeseer, 1995.
- [19] S. Z. Yong, B. Paden, and E. Frazzoli, "Computational methods for mimo flat linear systems: Flat output characterization, test and tracking control," in *2015 American Control Conference (ACC)*, pp. 3898–3904, IEEE, 2015.
- [20] D. Zanotto, G. Rosati, and S. Agrawal, "A higher-order method for dynamic optimization of controllable linear time-invariant systems," *Journal of Dynamic Systems, Measurement and Control, Transactions of the ASME*, vol. 135, no. 2, 2013.
- [21] J.-C. Ryu and S. K. Agrawal, "Differentially flat mobile manipulators mounted with an under-actuated vertical arm," in *2010 IEEE International Conference on Robotics and Automation*, pp. 5201–5206, IEEE, 2010.
- [22] H. Mounier and J. Rudolph, "Flatness and quasi-static state feedback in non-linear delay systems," *International Journal of Control*, vol. 81, no. 3, pp. 445–456, 2008.
- [23] J. Franch, S. Agrawal, and V. Sangwan, "Differential flatness of a class of n-dof planar manipulators driven by 1 or 2 actuators," *IEEE Transactions on Automatic Control*, vol. 55, no. 2, pp. 548–554, 2010.
- [24] J. Franch, À. Reyes, and S. K. Agrawal, "Differential flatness of a class of n—dof planar manipulators driven by an arbitrary number of actuators," in *2013 European Control Conference (ECC)*, pp. 161–166, IEEE, 2013.
- [25] V. Sangwan, H. Kuebler, and S. K. Agrawal, "Differentially flat design of under-actuated planar robots: Experimental results," in *2008 IEEE International Conference on Robotics and Automation*, pp. 2423–2428, IEEE, 2008.
- [26] M. Bottin and G. Rosati, "Comparison of under-actuated and fully actuated serial robotic arms: A case study," *Journal of Mechanisms and Robotics*, vol. 14, no. 3, p. 034503, 2022.
- [27] M. Tonan, A. Doria, M. Bottin, and G. Rosati, "Oscillation-free point-to-point motions of planar differentially flat under-actuated robots: a laplace transform method," *Robotica*, vol. 42, no. 4, p. 1262 – 1280, 2024.
- [28] M. Massaro, S. Lovato, M. Bottin, and G. Rosati, "An optimal control approach to the minimum-time trajectory planning of robotic manipulators," *Robotics*, vol. 12, no. 3, 2023.
- [29] G. Field and Y. Stepanenko, "Iterative dynamic programming: an approach to minimum energy trajectory planning for robotic manipulators," in *Proceedings of IEEE International Conference on Robotics and Automation*, vol. 3, pp. 2755–2760 vol.3, 1996.
- [30] L. E. Beaver and A. A. Malikopoulos, "Optimal control of differentially flat systems is surprisingly easy," *Automatica*, vol. 159, p. 111404, 2024.
- [31] F. A. Gomez Becerra, V. H. Olivares Peregrino, A. Blanco Ortega, and J. Linares Flores, "Optimal controller and controller based on differential flatness in a linear guide system: A performance comparison of indexes," *Mathematical Problems in Engineering*, vol. 2015, no. 1, p. 589184, 2015.
- [32] M. Tonan, M. Bottin, A. Doria, and G. Rosati, "Motion planning of differentially flat planar underactuated robots," *Robotics*, vol. 13, no. 4, 2024.
- [33] J. L. Troutman, *Variational calculus and optimal control: optimization with elementary convexity*. Springer Science & Business Media, 2012.